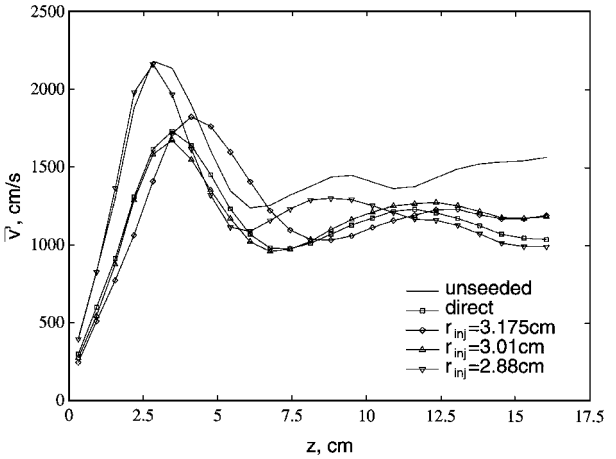

Fig. 3 Time-averaged rms fluctuating velocity in the shear layer as a function of downstream distance z for the unseeded flow, the direct simulation, and virtual particle simulations.

Finally, a Fourier analysis of velocity fluctuations in the shear layer indicates that in both the $r_{inj} = 3.01$ and 2.88 cm virtual particle simulations a downward shift in the vortex shedding frequency is observed with $\sigma_s = 1355$ and 1350 Hz, respectively. This shift is due to a thickening of the shear layer caused by the presence of a high concentration of particles injected at a lower velocity than the carrier fluid in the high-speed side of the shear layer. No such frequency shift was observed in either the direct simulation where particles are distributed uniformly across the shear layer or the virtual simulation with $r_{inj} = 3.175$ cm where the injection velocity is approximately the same as the gas phase in the core region of the shear layer.

Conclusions

Our investigation of a two-way coupled gas-particle system indicates that the shear-layer dynamics in a ramjet combustor can be modulated by controlling the dispersed-phase injection parameters, especially the particle injection location, size, velocity, and mass loading ratio. Both direct and virtual particle simulation techniques were employed to simulate the stream of particles injected into the shear-layer region. The effect of particle mass loading on the flow is seen as an attenuation of velocity fluctuations in the shear layer. In the direct simulations this attenuation is observed at all locations downstream of particle injection. When modeling the particle stream using the virtual particle method, attenuation is found to depend on injection location. The injection location corresponding to the central injection location of the particle stream, at $r_{inj} = 3.01$ cm, provides the best approximation to attenuation levels achieved in the direct case. When injecting at this location, though, dispersion was slightly underestimated because of reduced centrifugal effects. In addition, the choice of injection location was seen to alter slightly the characteristic vortex shedding frequency as the shear-layer thickness may be increased effectively by the presence of the particles. When taken in context, though, these results indicate that, when compared to the direct simulations, the virtual particle method can provide acceptable results and suggest that, with certain caveats, this technique can be used with confidence in situations where it is not practical to track every particle in the flow.

Acknowledgments

This work has been supported by the Office of Naval Research through the Mechanics and Energy Conversion Division and the U.S. Naval Research Laboratory. A grant of High Performance Computing (HPC) time from the Department of Defense HPC Shared Resource Center, U.S. Army Corps of Engineers Waterways Experiment Station is also gratefully acknowledged.

References

[1]Wang, L. P., and Maxey, M. R., "Settling Velocity and Concentration Distribution of Heavy Particles in Homogeneous Isotropic Turbulence," *Journal of Fluid Mechanics*, Vol. 256, 1993, pp. 27–68.

[2]Uthuppan, J., Aggarwal, S. K., Grinstein, F. F., and Kailasanath, K., "Particle Dispersion in a Transitional Axisymmetric Jet: A Numerical Simulation," *AIAA Journal*, Vol. 32, No. 10, 1994, pp. 2040–2048.

[3]Chang, E. J., and Kailasanath, K., "Simulations of Particle Dynamics in a Confined Shear Flow," *AIAA Journal*, Vol. 34, No. 6, 1996, pp. 1160–1166.

[4]Chang, E. J., and Kailasanath, K., "Behavior of Heavy Particles in an Acoustically Forced Confined Shear Flow," *AIAA Journal*, Vol. 34, No. 11, 1996, pp. 2429–2431.

[5]Raju, M. S., and Sirignano, W. A., "Spray Computations in a Centerbody Combustor," *Journal of Propulsion and Power*, Vol. 6, No. 2, 1990, pp. 97–105.

[6]Elghobashi, S. E., "On Predicting Particle-Laden Turbulent Flows," *Applied Scientific Research*, Vol. 52, No. 4, 1994, pp. 309–329.

[7]Boris, J. P., and Book, D. L., "Flux-Corrected Transport I: SHASTA—A Fluid Transport Algorithm That Works," *Journal of Computational Physics*, Vol. 11, 1973, pp. 38–69.

[8]Aggarwal, S. K., Fix, G., Lee, D. N., and Sirignano, W. A., "Numerical Optimization Studies of Axisymmetric Unsteady Sprays," *Journal of Computational Physics*, Vol. 50, No. 1, 1983, pp. 101–115.

[9]Squires, K. D., and Eaton, J. K., "Particle Response and Turbulence Modification in Isotropic Turbulence," *Physics of Fluids A*, Vol. 2, No. 7, 1990, pp. 1191–1203.

G. M. Faeth
Editor-in-Chief

Nonsingular Eigenvectors of the Flux Jacobian Matrix for Reactive Flow Problems

Mark A. Busby*
U.S. Naval Surface Warfare Center, Bethesda, Maryland 20817
and
Pasquale Cinnella†
Mississippi State University, Mississippi State, Mississippi 39762

I. Introduction

THE development of numerical tools for the simulation of finite-rate chemistry flows has received increasing attention over the past decade. Reacting flows play an important role in a wide range of scientific fields, such as combustion, hypersonic flight, and explosion analysis. The purpose of this study is to describe a step that can be taken to develop accurate and efficient solutions for such flows: The eigensystem of the Euler equations for a flow in chemical nonequilibrium is developed, including a well-designed set of eigenvectors for higher-order upwind applications, which do not contain potentially ill-defined terms. This work results in an extension of the methods developed by Whitfield and Janus[1] for a perfect gas and their later extensions.[2]

Several researchers have developed upwind, implicit, finite-rate chemistry algorithms for very general flow situations. References 3–5 are representative of the currently available technology. A common thread among these solvers is the development and use of eigenvalues and eigenvectors of the inviscid fluxes, which are necessary for the design of the numerical schemes. The choice of eigenvectors is somewhat arbitrary because of the presence of repeated eigenvalues. The eigensystem proposed by Cinnella,[6] although ideally suited when used with higher-order spatially accurate MUSCL schemes, can prove inadequate when used in conjunction with flux-extrapolation schemes. (The MUSCL approach achieves high-order

Received July 25, 1998; revision received Nov. 16, 1998; accepted for publication Nov. 25, 1998.

*Mathematician, Carderock Division. Member AIAA.
†Associate Professor, Department of Aerospace Engineering. Senior Member AIAA.

accuracy in space by reconstructing the fluxes at cell faces using extrapolations of appropriate flow variables. This should be contrasted with the flux-extrapolation technique, whereby the fluxes are extrapolated directly to the cell faces.) The reason for this possible inadequacy is rooted in the occurrence of species mass fractions in the denominator of elements in the matrix of left eigenvectors, which can cause large values when computing trace elements (where species density is very small) and can lead to numerical convergence problems. Unlike the MUSCL approach, flux extrapolation techniques require the matrix of left eigenvectors. This study focuses on the development of an eigensystem that can be applied safely for flux-extrapolation upwinding schemes, as well as MUSCL methodologies.

II. Physical Model

The equations that govern chemically reacting flows are written in integral form for a gas mixture containing NS distinct species. For an arbitrary nondeforming volume $\mathcal{V}$, closed by a boundary $\mathcal{S}$, they read

$$\frac{\partial}{\partial t}\iiint_{\mathcal{V}} \boldsymbol{Q}\,\mathrm{d}\mathcal{V} + \oint_{\mathcal{S}} \boldsymbol{S}\cdot\boldsymbol{n}\,\mathrm{d}\mathcal{S} = \iiint_{\mathcal{V}} \boldsymbol{W}\,\mathrm{d}\mathcal{V} \tag{1}$$

where $\boldsymbol{Q}$ is the vector of conserved variables, $\boldsymbol{S}$ is the inviscid flux vector, and $\boldsymbol{W}$ is the vector of source terms. The unit vector $\boldsymbol{n}$ is normal to the infinitesimal area $\mathrm{d}\mathcal{S}$ and points outward. Utilizing a Cartesian frame of reference (x, y, z) whose unit vectors are $\boldsymbol{i}$, $\boldsymbol{j}$, and $\boldsymbol{k}$, respectively, the vectors $\boldsymbol{Q}$, $\boldsymbol{S}$, and $\boldsymbol{W}$ read

$$\boldsymbol{Q} = \begin{bmatrix} \rho_1 \\ \rho_2 \\ \vdots \\ \rho_{NS} \\ \rho u \\ \rho v \\ \rho w \\ \rho e_0 \end{bmatrix}, \qquad \boldsymbol{S} = \begin{bmatrix} \rho_1 \boldsymbol{u} \\ \rho_2 \boldsymbol{u} \\ \vdots \\ \rho_{NS} \boldsymbol{u} \\ \rho u \boldsymbol{u} + p\boldsymbol{i} \\ \rho v \boldsymbol{u} + p\boldsymbol{j} \\ \rho w \boldsymbol{u} + p\boldsymbol{k} \\ (\rho e_0 + p)\boldsymbol{u} \end{bmatrix}, \qquad \boldsymbol{W} = \begin{bmatrix} w_1 \\ w_2 \\ \vdots \\ w_{NS} \\ 0 \\ 0 \\ 0 \\ 0 \end{bmatrix} \tag{2}$$

In the preceding formulas $\rho = \sum \rho_i$ is the density of the gas, sum of the species values ρ_i; e_0 is the total energy per unit mass; and p is the pressure. Moreover, the mixture velocity $\boldsymbol{u}$, whose Cartesian components are (u, v, w), has been utilized. The first NS equations are species continuity equations, relating the time rate of change of species densities ρ_s to convective and diffusive transport and to the creation/destruction of the species due to chemical reactions. The species rates of production w_s are given by Busby and Cinnella.[7] Following species continuity are the three components of the momentum equation. Finally, the global energy equation describes the time evolution of the total internal energy per unit volume ρe_0:

$$\rho e_0 = \rho e + \rho\frac{q^2}{2}, \qquad \rho e = \sum_{i=1}^{NS} \rho_i e_i(T)$$
$$q^2 = u^2 + v^2 + w^2 \tag{3}$$

where e_i are the species internal energies per unit mass, which are functions of temperature only.[8] The system is closed by a thermal equation of state, given by

$$p = \sum_{i=1}^{NS} \rho_i R_i T \tag{4}$$

where R_i is the species gas constant and T is the mixture temperature.

Finally, the frozen speed of sound can be found easily for a mixture of thermally perfect gases.[8] It reads

$$a = \sqrt{\gamma(p/\rho)} \tag{5}$$

where γ is the mixture ratio of frozen specific heats.

III. Eigensystem

The system of equations developed in the preceding section is nonlinear and coupled and can be written in various equivalent forms. In particular a differential conservative form can be derived for generalized fixed curvilinear coordinates, as follows[6]:

$$\frac{\partial}{\partial t}\left(\frac{\boldsymbol{Q}}{J}\right) + \frac{\partial \tilde{\boldsymbol{F}}}{\partial \xi} + \frac{\partial \tilde{\boldsymbol{G}}}{\partial \eta} + \frac{\partial \tilde{\boldsymbol{H}}}{\partial \zeta} = \frac{\boldsymbol{W}}{J} \tag{6}$$

where $\boldsymbol{Q}$ is the vector of conserved variables and $\boldsymbol{W}$ is the vector of production rates, already defined in Eq. (2), and the inviscid flux vectors are $\tilde{\boldsymbol{F}}$, $\tilde{\boldsymbol{G}}$, and $\tilde{\boldsymbol{H}}$, with $\tilde{\boldsymbol{F}}$ given as

$$\tilde{\boldsymbol{F}} = (|\nabla\xi|/J)[\rho_1\tilde{u}, \rho_2\tilde{u}, \ldots, \rho_{NS}\tilde{u}, \rho u\tilde{u} + \tilde{\xi}_x p,$$
$$\rho v\tilde{u} + \tilde{\xi}_y p, \rho w\tilde{u} + \tilde{\xi}_z p, \tilde{u}(\rho e_0 + p)]^T \tag{7}$$

and $\tilde{\boldsymbol{G}}$ and $\tilde{\boldsymbol{H}}$ given by similar expressions, once the appropriate contravariant velocity components and generalized coordinates are chosen. In the preceding equations J is the Jacobian of the transformation between curvilinear and Cartesian coordinates, and $\tilde{u}$, $\tilde{v}$, $\tilde{w}$ are the contravariant velocity components

$$\begin{bmatrix} \tilde{u} \\ \tilde{v} \\ \tilde{w} \end{bmatrix} = \begin{bmatrix} \tilde{\xi}_x & \tilde{\xi}_y & \tilde{\xi}_z \\ \tilde{\eta}_x & \tilde{\eta}_y & \tilde{\eta}_z \\ \tilde{\zeta}_x & \tilde{\zeta}_y & \tilde{\zeta}_z \end{bmatrix} \begin{bmatrix} u \\ v \\ w \end{bmatrix} \tag{8}$$

where the normalized gradients in the ξ, η, and ζ directions have been utilized. Alternatively, a set of primitive variables can be introduced:

$$\boldsymbol{q} = [\rho_1, \rho_2, \ldots, \rho_{NS}, u, v, w, p]^T \tag{9}$$

which is often used to develop physical boundary conditions necessary for the numerical solution of the Euler equations.[9]

The development of the eigensystem of the flux Jacobians will be discussed next. The intent is to develop eigenvectors that do not feature any singularities for cases where some of the species in the gas mixture are present in trace amounts and that can be used for both MUSCL[9] and flux extrapolation[2] space discretizations. The result also can be employed to develop a set of characteristic equations and the resulting characteristic variable boundary conditions, as shown in Ref. 10.

A. Eigenvalues

The three-dimensional Euler equations can be cast in quasilinear form as follows:

$$\frac{\partial}{\partial t}\left(\frac{\boldsymbol{Q}}{J}\right) + \frac{\partial \tilde{\boldsymbol{F}}}{\partial \boldsymbol{Q}}\frac{\partial \boldsymbol{Q}}{\partial \xi} + \frac{\partial \tilde{\boldsymbol{G}}}{\partial \boldsymbol{Q}}\frac{\partial \boldsymbol{Q}}{\partial \eta} + \frac{\partial \tilde{\boldsymbol{H}}}{\partial \boldsymbol{Q}}\frac{\partial \boldsymbol{Q}}{\partial \zeta} = \frac{\boldsymbol{W}}{J} \tag{10}$$

or

$$\frac{\partial}{\partial t}\left(\frac{\boldsymbol{Q}}{J}\right) + \tilde{\boldsymbol{A}}\frac{\partial \boldsymbol{Q}}{\partial \xi} + \tilde{\boldsymbol{B}}\frac{\partial \boldsymbol{Q}}{\partial \eta} + \tilde{\boldsymbol{C}}\frac{\partial \boldsymbol{Q}}{\partial \zeta} = \frac{\boldsymbol{W}}{J} \tag{11}$$

In Eq. (11) $\tilde{\boldsymbol{A}}$, $\tilde{\boldsymbol{B}}$, and $\tilde{\boldsymbol{C}}$ are the flux Jacobian matrices, which are given in Ref. 10. In the following, when a generic direction k is considered (which can be ξ, η, or ζ), the corresponding flux vector will be denoted by $\tilde{\boldsymbol{S}}$ and its Jacobian matrix will be $\tilde{\boldsymbol{K}} = \partial\tilde{\boldsymbol{S}}/\partial\boldsymbol{Q}$. Matrix $\tilde{\boldsymbol{K}}$ turns out to be dense and not easily amenable to algebraic manipulation. On the other hand, working with the primitive variables already introduced simplifies considerably the task of finding the eigensystem of the flux Jacobians. Transforming Eq. (11) from conservative to primitive variables results in the following:

$$\frac{\partial \boldsymbol{Q}}{\partial \boldsymbol{q}}\frac{\partial}{\partial t}\left(\frac{\boldsymbol{q}}{J}\right) + \tilde{\boldsymbol{A}}\frac{\partial \boldsymbol{Q}}{\partial \boldsymbol{q}}\frac{\partial \boldsymbol{q}}{\partial \xi} + \tilde{\boldsymbol{B}}\frac{\partial \boldsymbol{Q}}{\partial \boldsymbol{q}}\frac{\partial \boldsymbol{q}}{\partial \eta} + \tilde{\boldsymbol{C}}\frac{\partial \boldsymbol{Q}}{\partial \boldsymbol{q}}\frac{\partial \boldsymbol{q}}{\partial \zeta} = \frac{\boldsymbol{W}}{J} \tag{12}$$

where the transformation between the conserved and primitive variables is defined by $\boldsymbol{M} = \partial \boldsymbol{Q}/\partial \boldsymbol{q}$ and can be found easily.[7,10] Moreover, its inverse, $\boldsymbol{M}^{-1}$, can be computed directly with little difficulty.[7,10]

Multiplying Eq. (12) by $\boldsymbol{M}^{-1}$ yields

$$\frac{\partial}{\partial t}\left(\frac{\boldsymbol{q}}{J}\right) + \boldsymbol{M}^{-1}\tilde{\boldsymbol{A}}\boldsymbol{M}\frac{\partial \boldsymbol{q}}{\partial \xi} + \boldsymbol{M}^{-1}\tilde{\boldsymbol{B}}\boldsymbol{M}\frac{\partial \boldsymbol{q}}{\partial \eta} + \boldsymbol{M}^{-1}\tilde{\boldsymbol{C}}\boldsymbol{M}\frac{\partial \boldsymbol{q}}{\partial \zeta} = \boldsymbol{M}^{-1}\frac{\boldsymbol{W}}{J} \tag{13}$$

where a similarity transformation relates the generic Jacobian matrix $\tilde{\boldsymbol{K}}$ to the matrix $\tilde{\boldsymbol{k}}$, as follows:

$$\tilde{\boldsymbol{k}} = \boldsymbol{M}^{-1}\tilde{\boldsymbol{K}}\boldsymbol{M} \tag{14}$$

Unlike $\tilde{\boldsymbol{K}}$, the matrix $\tilde{\boldsymbol{k}}$ turns out to be sparse and easy to use.[1,7] The eigenvalues of $\tilde{\boldsymbol{k}}$ can be found with relative ease and are

$$\lambda_1 = \lambda_2 = \cdots = \lambda_{NS+2} = (|\nabla k|/J)\tilde{u}$$
$$\lambda_{NS+3} = (|\nabla k|/J)(\tilde{u} + a), \qquad \lambda_{NS+4} = (|\nabla |k/J)(\tilde{u} - a) \tag{15}$$

Because of the similarity transformation [Eq. (14)], the eigenvalues of $\tilde{\boldsymbol{K}}$ are also given by Eq. (15).

B. Eigenvectors

A set of linearly independent eigenvectors can be developed for the Jacobian matrix $\tilde{\boldsymbol{k}}$. This set must be chosen carefully because of the presence of repeated eigenvalues. The development is similar to that followed by Whitfield and Janus.[1] The final matrix of right eigenvectors reads

$$\boldsymbol{P}_k = \begin{bmatrix} \alpha & \cdots & 0 & \alpha_1\tilde{k}_y & \alpha_1\tilde{k}_z & \alpha_1 & \alpha_1 \\ \vdots & \ddots & \vdots & \vdots & \vdots & \vdots & \vdots \\ 0 & \cdots & \alpha & \alpha_{NS}\tilde{k}_y & \alpha_{NS}\tilde{k}_z & \alpha_{NS} & \alpha_{NS} \\ 0 & \cdots & 0 & -\tilde{k}_z & \tilde{k}_y & \tilde{k}_x/\sqrt{2} & -\tilde{k}_x/\sqrt{2} \\ \tilde{k}_z & \cdots & \tilde{k}_z & 0 & -\tilde{k}_x & \tilde{k}_y/\sqrt{2} & -\tilde{k}_y/\sqrt{2} \\ -\tilde{k}_y & \cdots & -\tilde{k}_y & \tilde{k}_x & 0 & \tilde{k}_z/\sqrt{2} & -\tilde{k}_z/\sqrt{2} \\ 0 & \cdots & 0 & 0 & 0 & \alpha a^2 & \alpha a^2 \end{bmatrix} \tag{16}$$

where

$$\alpha_i = \rho_i/\sqrt{2}a, \qquad \alpha = \rho/\sqrt{2}a \tag{17}$$

The matrix of left eigenvectors can be found by inverting the preceding matrix. The final result reads

$$\boldsymbol{P}_k^{-1} = \begin{bmatrix} \dfrac{\alpha\beta - \alpha_1\left(1-\tilde{k}_x^2\right)}{\alpha^2\beta} & \cdots & \dfrac{-\alpha_1\left(1-\tilde{k}_x^2\right)}{\alpha^2\beta} & 0 & \dfrac{\alpha_1\tilde{k}_z}{\alpha\beta} & \dfrac{-\alpha_1\tilde{k}_y}{\alpha\beta} & \dfrac{-\alpha_1\tilde{k}_x}{\alpha^2\beta a^2} \\ \vdots & \ddots & \vdots & \vdots & \vdots & \vdots & \vdots \\ \dfrac{-\alpha_{NS}\left(1-\tilde{k}_x^2\right)}{\alpha^2\beta} & \cdots & \dfrac{\alpha\beta - \alpha_{NS}\left(1-\tilde{k}_x^2\right)}{\alpha^2\beta} & 0 & \dfrac{\alpha_{NS}\tilde{k}_z}{\alpha\beta} & \dfrac{-\alpha_{NS}\tilde{k}_y}{\alpha\beta} & \dfrac{-\alpha_{NS}\tilde{k}_x}{\alpha^2\beta a^2} \\ \dfrac{\tilde{k}_y}{\alpha\beta} & \cdots & \dfrac{\tilde{k}_y}{\alpha\beta} & -\tilde{k}_z & \dfrac{-\tilde{k}_y\tilde{k}_z(1-\tilde{k}_x)}{\beta} & \dfrac{1-\tilde{k}_z^2(1-\tilde{k}_x)}{\beta} & \dfrac{-\tilde{k}_y}{\alpha\beta a^2} \\ \dfrac{\tilde{k}_z}{\alpha\beta} & \cdots & \dfrac{\tilde{k}_z}{\alpha\beta} & \tilde{k}_y & \dfrac{-1+\tilde{k}_y^2(1-\tilde{k}_x)}{\beta} & \dfrac{\tilde{k}_y\tilde{k}_z(1-\tilde{k}_x)}{\beta} & \dfrac{-\tilde{k}_z}{\alpha\beta a^2} \\ 0 & \cdots & 0 & \tilde{k}_x/\sqrt{2} & \tilde{k}_y/\sqrt{2} & \tilde{k}_z/\sqrt{2} & 1/2\alpha a^2 \\ 0 & \cdots & 0 & -\tilde{k}_x/\sqrt{2} & -\tilde{k}_y/\sqrt{2} & -\tilde{k}_z/\sqrt{2} & 1/2\alpha a^2 \end{bmatrix} \tag{18}$$

where

$$\beta = \tilde{k}_x + \tilde{k}_y^2 + \tilde{k}_z^2 \tag{19}$$

Because of the similarity of matrices $\tilde{\boldsymbol{K}}$ and $\tilde{\boldsymbol{k}}$ [see Eq. (14)], their eigenvalues are the same, and their eigenvectors are related. The right and left eigenvector matrices for $\tilde{\boldsymbol{K}}$ (denoted by $\boldsymbol{T}_k$ and $\boldsymbol{T}_k^{-1}$, respectively) can be found from the following:

$$\boldsymbol{T}_k = \boldsymbol{M}\boldsymbol{P}_k, \qquad \boldsymbol{T}_k^{-1} = \boldsymbol{P}_k^{-1}\boldsymbol{M}^{-1} \tag{20}$$

The full matrices are presented in Ref. 7.

IV. Numerical Approach

The system of equations that describes compressible, inviscid, chemically reacting flows must be discretized to form a set of algebraic equations that can be solved computationally. The discretization of the equations is an extension of the methods used by Whitfield et al.[2] The general methods used also have been discussed for chemically reacting flows by Cinnella.[6]

V. Numerical Results

Numerical results for a few test cases have been obtained to investigate the space discretization based on the new eigensystem of the inviscid fluxes. Only one result will be discussed here; the interested reader can find more in Ref. 10.

The test case represents inviscid, steady flow. For reacting flow, initial freestream conditions are given as a fluid in thermodynamic and chemical equilibrium. The ONERA M6 wing at a freestream Mach number of $M_\infty = 0.84$ and an angle of attack of -3.06 deg is considered a standard transonic test case. In this study the wing is used to validate the new eigensystem by comparison with the perfect gas code by Whitfield et al.,[2] developed for upwind, flux-difference split, high-resolution space discretizations. The current simulations use a five-species/17-reaction air model[7] with a freestream temperature of 300 K and pressure of one atmosphere and a frozen model that does not include chemical kinetics. Initial equilibrium values are computed based on a mixture of approximately 79% N_2 and 21% O_2. A coarse $49 \times 9 \times 9$ grid is used. The simulation is run with second-order spatial accuracy and a fully implicit time integration scheme, using a minmod limiter and a fixed Courant–Friedrichs–Lewy number of 7.5.

Figure 1 shows excellent agreement between the two codes for the pressure distribution at the midspan of the wing. Similar results apply for the drag coefficient and all other flow properties.[7,10] No numerical difficulties or unexpected behavior are recorded for this case, even if some of the chemical species are present in extremely small quantities (mass fractions at the round-off level for atomic oxygen and nitrogen).

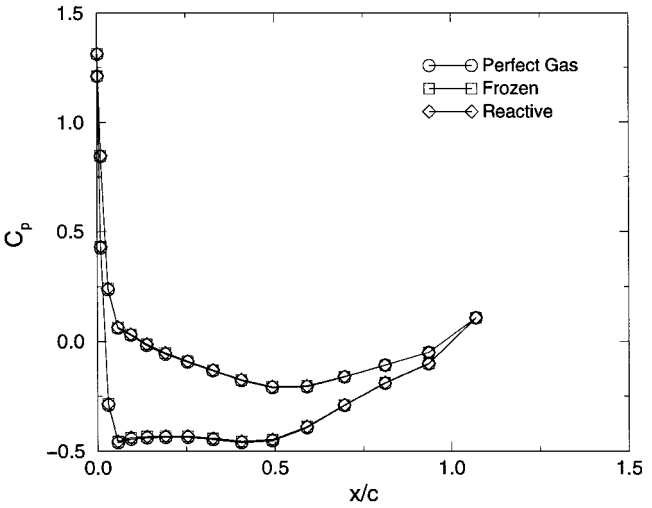

Fig. 1 Comparison of pressure coefficient predictions for M6 Onera wing at $M_\infty = 0.84$.

VI. Conclusion

The purpose of this study was to develop an eigensystem of the inviscid flux Jacobians that does not contain singularities and can be used to compute flows with finite-rate chemistry using spatially accurate methods. The eigensystem developed is valid for both flux extrapolation and dependent-variable extrapolation, higher-order-accurate extensions to the flux vector-difference scheme developed by Roe.

Acknowledgments

This work was supported in part by the National Science Foundation, which funds the Engineering Research Center for Computational Field Simulation at Mississippi State University, and by the In-House Library Independent Research Program at Carderock Division, U.S. Naval Surface Warfare Center.

References

[1]Whitfield, D. L., and Janus, J. M., "Three-Dimensional Unsteady Euler Equations Solution Using Flux Vector Splitting," AIAA Paper 84-1552, June 1984.

[2]Whitfield, D. L., Janus, J. M., and Simpson, L. B., "Implicit Finite Volume High Resolution Wave-Split Scheme for Solving the Unsteady Three-Dimensional Euler and Navier–Stokes Equations on Stationary or Dynamic Grids," Dept. of Aerospace Engineering, Rept. MSSU-EIRS-ASE-88-2, Mississippi State Univ., Mississippi State, MS, Feb. 1988.

[3]Walters, R. W., Cinnella, P., Slack, D., and Halt, D., "Characteristic-Based Algorithms for Flows in Thermochemical Nonequilibrium," *AIAA Journal*, Vol. 30, No. 5, 1992, pp. 1304–1313.

[4]Hosangadi, A., Sinha, N., and Dash, S. M., "Multi-Dimensional Simulation of ETC Gun Flowfields," U.S. Army Research Lab., Rept. ARL-CR-240, Fort Washington, PA, Aug. 1995.

[5]Liu, Y., and Vinokur, M., "Upwind Algorithms for General Thermo-Chemical Nonequilibrium Flows," AIAA Paper 89-0201, Jan. 1989.

[6]Cinnella, P., "Flux-Split Algorithms for Flows with Non-Equilibrium Chemistry and Thermodynamics," Ph.D. Dissertation, Dept. of Aerospace and Ocean Engineering, Virginia Polytechnic Inst. and State Univ., Blacksburg, VA, Dec. 1989.

[7]Busby, M. A., and Cinnella, P., "Steps Toward More Accurate and Efficient Simulations of Reactive Flows," AIAA Paper 98-2425, July 1998.

[8]Vincenti, W. G., and Kruger, C. H., Jr., *Introduction to Physical Gas Dynamics*, Krieger, Malabar, FL, 1965, Chap. 4.

[9]Hirsch, C., *Numerical Computation of Internal and External Flows*, Vol. 2, Wiley, New York, 1990, Chaps. 19, 20.

[10]Busby, M. A., "Steps Toward More Accurate and Efficient Simulations of Reactive Flows," Ph.D. Dissertation, Dept. of Aerospace Engineering, Mississippi State Univ., Mississippi State, MS, Aug. 1997.

K. Kailasanath
Associate Editor

Instantaneous Velocity Measurements Around an Oscillating Airfoil

Mark Rank*
University of Wisconsin–Platteville, Platteville, Wisconsin 53818-3099
and
B. R. Ramaprian†
Washington State University, Pullman, Washington 99164-2920

Introduction

THE study of vortex dynamics and stall associated with oscillating airfoils has been a topic of fundamental research in the aerodynamics community for many years. The details of the dynamic stall process[1] strongly depend on the airfoil geometry, the oscillation amplitude $\Delta\alpha$, the maximum incidence α_{max}, and the reduced frequency $k\ (=\pi fc/U_\infty)$, where f is the oscillation frequency, c the airfoil chord, and U_∞ the freestream velocity. McCroskey[1] identified two categories of dynamic stall, namely light stall and deep stall. Light dynamic stall, which occurs at relatively smaller values of k and moderate values of $\Delta\alpha$ and α_{max}, shares many of the features of static stall but in addition results in large hysteresis effects on aerodynamic loading. Deep dynamic stall, on the other hand, is characterized primarily by the shedding of a dynamic stall vortex (DSV). This type of stall, which occurs at larger values of k, $\Delta\alpha$, and α_{max}, leads not only to large hysteresis loops as in the light-stall case but also to very large variations in aerodynamic loading during the oscillation cycle caused by the buildup and shedding of the DSV. The present work was directed at the study of airfoil oscillation at $k = 0.05$, under which conditions the flow is expected to be characterized by light stall, in the sense just defined.

There have been several flow-visualization studies reported on the dynamic stall of oscillating airfoils. There are also extensive data on surface pressure and aerodynamic coefficients for both light and deep dynamic stall conditions. However, to the best of the authors' knowledge, there has been only one reported experiment[2] in which the instantaneous velocity field was measured on an oscillating airfoil, using the technique of particle image velocimetry (PIV). That experiment was performed at a high k value of about 0.2, at which deep stall conditions were observed. The present work represents a complementary effort to obtain data under conditions of light dynamic stall.

Description of the Experiment

This study was conducted in the large water channel facility at Washington State University. This is the same facility in which earlier dynamic stall studies have been performed in recent years. The flow facility is a 1 m wide × 0.67 m deep (3 × 2 ft) closed-loop open surface water channel. A two-dimensional NACA 0015 airfoil of 300-mm (1-ft) chord and 600-mm (2-ft) span was mounted vertically from a platform in such a way that, when rotated, the airfoil would pitch about its quarter-chord axis. The submerged end of the airfoil was fitted with an end plate to reduce end effects. This flow facility and experimental arrangement have been used extensively in the past for the study of dynamic stall of airfoils pitching at constant

Received May 2, 1998; revision received Oct. 21, 1998; accepted for publication Nov. 6, 1998.

*Database Administrator, Office of Information Technology. Member AIAA.

†Professor, School of Mechanical and Materials Engineering. Member AIAA.